Accepted ApJL 02 May 2008
Preprint typeset using LaTeX style emulateapj v. 11/12/01

arXiv:0805.0321v1 [astro-ph] 2 May 2008

MOLECULAR GAS IN THE z=1.2 ULTRALUMINOUS MERGER GOODS J123634.53+621241.3

David T. Frayer[1], Jin Koda[2], Alexandra Pope[3,4], Minh T. Huynh[1], Ranga-Ram Chary[5], Douglas Scott[6], Mark Dickinson[4], Douglas C.-J. Bock[7], John M. Carpenter[2], David Hawkins[8], Mark Hodges[8], James W. Lamb[8], Richard L. Plambeck[9], Marc W. Pound[10], Stephen L. Scott[8], Nicholas Z. Scoville[2], and David P. Woody[8]

Accepted ApJL 02 May 2008

ABSTRACT

We report the detection of CO(2→1) emission from the $z = 1.2$ ultraluminous infrared galaxy (ULIRG) GOODS J123634.53+621241.3 (also known as the sub-millimeter galaxy GN26). These observations represent the first discovery of high-redshift CO emission using the new Combined Array for Research in Millimeter-Wave Astronomy (CARMA). Of all high-redshift ($z > 1$) galaxies within the GOODS-North field, this source has the largest far-infrared (FIR) flux observed in the *Spitzer* 70 μm and 160 μm bands. The CO redshift confirms the optical identification of the source, and the bright CO(2→1) line suggests the presence of a large molecular gas reservoir of about $7 \times 10^{10} M_{\odot}$. The infrared-to-CO luminosity ratio of $L(\mathrm{IR})/L'(\mathrm{CO}) = 80 \pm 30\,\mathrm{L}_{\odot}(\mathrm{K\,km\,s^{-1}\,pc^2})^{-1}$ is slightly smaller than the average ratio found in local ULIRGs and high-redshift sub-millimeter galaxies. The short star-formation time scale of about 70 Myr is consistent with a starburst associated with the merger event and is much shorter than the time scales for spiral galaxies and estimates made for high-redshift galaxies selected on the basis of their $B - z$ and $z - K$ colors.

Subject headings: galaxies: evolution — galaxies: formation — galaxies: individual (GOODS J123634.53+621241.3) — galaxies: starburst

1. INTRODUCTION

Observations of molecular gas are fundamental to our understanding of galaxy evolution by providing measurements of the material from which stars form. The discovery of sub-millimeter galaxies (SMGs, Smail et al. 1997; Hughes et al. 1998; Barger et al. 1998) enabled the ability to measure the molecular CO properties of the most luminous infrared sources at high-redshift (Frayer et al. 1998, 1999; Neri et al. 2003; Greve et al. 2005; Tacconi et al. 2006, 2008). These observations have shown that the CO properties of the SMGs are similar to local ultraluminous infrared galaxies (ULIRGs, $L_{\mathrm{IR}} > 10^{12}\,L_{\odot}$), and their number densities indicate that ULIRGs are 1000 times more common at $z \sim 2$ than locally (Chapman et al. 2005). The importance of ULIRGs at high-redshift has been reinforced by deep *Spitzer* mid-infrared (MIR) surveys at 24 μm (e.g., Chary et al. 2004; Lagache et al. 2004). At $z \sim$ 1–2, the majority of star-formation and AGN activity occurs within dust-rich luminous infrared galaxies (Le Floc'h et al. 2005; Papovich et al. 2006; Caputi et al. 2007).

Although the bulk of the infrared luminosity of galaxies arises in the rest-frame far-infrared band (FIR, 40–120 μm), this band has been mostly unexplored at high-redshift. The majority of high-redshift ULIRGs have been identified by 24 μm and sub-mm/mm surveys. These surveys yield highly uncertain bolometric corrections for the infrared luminosity. Deep surveys at 70 μm and 160 μm with *Spitzer* enable the direct identification of luminous sources within the FIR band. In this Letter we report on CO observations of the brightest FIR source at $z > 1$ in GOODS-North. The source GOODS J123634.53+621241.3 (also known as SMG GN26) was identified as being unusually bright at 70 & 160 μm (Frayer et al. 2006; Huynh et al. 2007) and for having strong emission from polycyclic aromatic hydrocarbon (PAH) molecules (Pope et al. 2008). At optical wavelengths, GN26 has a merger-like morphology with a disturbed core and evidence of tidal tails on larger scales. Although it has a large FIR flux, it is among the faintest 850 μm sources detected to date (Borys et al. 2003; Pope et al. 2006). A cosmology of $h_{70} \equiv \mathrm{H}_0(70\,\mathrm{km\,s^{-1}\,Mpc^{-1}})^{-1} = 1$, $\Omega_{\mathrm{M}} = 0.3$, and $\Omega_{\Lambda} = 0.7$ is assumed throughout this paper.

2. OBSERVATIONS

The CO(2→1) observations of GN26 were taken between 2007 April 14 – June 28 with the Combined Array for Research in Millimeter-Wave Astronomy (CARMA) in the low-resolution D-configuration, resulting in a to-

---

[1] Infrared Processing and Analysis Center, California Institute of Technology 100-22, Pasadena, CA 91125, USA; frayer@ipac.caltech.edu
[2] Astronomy Department, California Institute of Technology 105–24, Pasadena, CA 91125, USA
[3] *Spitzer* Fellow
[4] National Optical Astronomy Observatory, 950 N. Cherry Ave., Tucson, AZ, 85719, USA
[5] *Spitzer* Science Center, California Institute of Technology 220-6, Pasadena, CA 91125, USA
[6] Department of Physics & Astronomy, University of British Columbia, Vancouver, BC, V6T 1Z1, Canada
[7] Combined Array for Research in Millimeter-wave Astronomy, P.O Box 968, Big Pine, CA 93513, USA
[8] Owens Valley Radio Observatory, California Institute of Technology, Big Pine, CA 93513, USA
[9] Department of Astronomy and Radio Astronomy Laboratory, University of California, Berkeley, CA 94720, USA
[10] Department of Astronomy, University of Maryland, College Park, MD 20742, USA

tal of 26.4 hours of on-source data. The adopted phase center was the IRAC position of α(J2000)=$12^{\mathrm{h}}36^{\mathrm{m}}34\overset{\mathrm{s}}{.}5$, δ(J2000)=$+62^{\circ}12'41''$ (Pope et al. 2006). The CO line was observed using a digital correlator configured with two adjacent 13×31.25 MHz bands centered on 103.89274 GHz in the upper side-band, corresponding to CO(2→1) emission at the reported optical redshift of $z = 1.219$ (Cohen et al. 1996). The nearby quasar J1153+495 (14° from GN26) was observed every 15 minutes for amplitude and phase calibration, and the bright quasars 3C 273, 3C 345, and J0927+390 were used for passband calibration and pointing. We estimate an uncertainty of 14% for the absolute calibration scale based on the observations of 3C 273 and 3C 345.

The data were reduced and calibrated using the Multichannel Image Reconstruction, Image Analysis, and Display (MIRIAD) software package (Sault et al. 1995). An interactive UV-plotting tool was used to visualize and flag spurious visibilities per baseline (105 baselines in total). Figure 1 shows the "dirty" (no cleaning) natural-weighted integrated CO(2→1) map made by averaging over the 10 channels showing CO emission at the phase center. No improvement in image quality was made using clean algorithms since the side-lobes are weaker than the noise due to the large number of baselines. The data are consistent with an unresolved point source. The weak tail extending eastward is not currently significant (Fig. 1). Higher resolution data with higher signal-to-noise would be needed to measure the CO morphology of the source.

3. RESULTS

The total CO(2→1) line flux of 3.45 ± 0.46 Jy km s^{-1} was derived from the integrated CO map (7.5σ, Fig. 1). The CO position and the limit to the CO source size of $< 4''$ (33 kpc) were derived from a "robust"-weighted image (ROBUST= 0). The derived position is consistent with previous optical and radio positions. The CO emission peaks at the central location of the merger event. With the current sensitivity and resolution, there is no evidence for CO emission from the nearby companion galaxy GOODS J123634.69+621243.7 at $z = 1.225$ (Cowie et al. 2004), which is about $3''$ north-east of GN26.

Figure 2 shows the CO(2→1) spectrum at the peak of the CO image. The spectrum was Hanning-smoothed for display purposes, but a Gaussian fit of the un-smoothed data was used to derive the CO redshift and line width (Table 1). The CO redshift of $z(\mathrm{CO}) = 1.2234 \pm 0.0007$ is slightly red-ward (600 km s^{-1}) of the reported optical redshift of $z = 1.219$ (Cohen et al. 1996; Cowie et al. 2004), which is not unusual for dust-obscured ultra-luminous systems (Frayer et al. 1999; Greve et al. 2005). Wirth et al. (2004) observed the galaxy with the Keck DEIMOS spectrograph but did not report a redshift. However, visual inspection of the spectrum using the Team Keck Treasury Redshift Survey on-line database shows an emission line consistent with [OII] λ3727Å at a redshift of $z = 1.224 \pm 0.001$, which agrees well with the measured CO redshift. In addition, the CO redshift is consistent with the redshift based on the PAH lines ($z = 1.23 \pm 0.01$) observed with *Spitzer* IRS (Pope et al. 2008). Based on its sub-mm and radio flux densities (S850 = 2.2 mJy; S1.4 GHz = 0.19 mJy, Pope et al. 2006), the continuum level at 3 mm is expected to be less than about 0.05 mJy. As expected, no continuum was detected from the co-addition of the lower and upper side-band line-free channels; S(3mm)$<$ 0.66 mJy (3σ). Since the 3 mm continuum level is negligible in comparison to the strong CO line, no continuum was subtracted from the data.

The observed CO(2→1) line flux implies an intrinsic CO line luminosity of $L'[\mathrm{CO}(2-1)] = (6.8 \pm 1.8) \times 10^{10}\,\mathrm{K\,km\,s^{-1}\,pc^{2}}$ (see formulae in Solomon & Vanden Bout 2005), which is a factor of 150–200 times larger than that for our Galaxy. The CO luminosity is related to the mass of molecular gas (including He) by $M(\mathrm{H}_2)/L'(\mathrm{CO}) = \alpha$. Given that Tacconi et al. (2008) have found that the conversion factor α for the SMGs is similar to that derived for local ULIRGs, we have adopted the average ULIRG value for GN26. Assuming $\alpha(1-0) = 0.8\,M_{\odot}(\mathrm{K\,km\,s^{-1}\,pc^{2}})^{-1}$ and $L'[\mathrm{CO}(2-1)]/L'[\mathrm{CO}(1-0)] \simeq 0.8$ as found for local ULIRGs (Downes & Solomon 1998), we adopt $\alpha(2-1) = 1\,M_{\odot}(\mathrm{K\,km\,s^{-1}\,pc^{2}})^{-1}$; i.e., $\alpha(2-1) = \alpha(1-0)(L'[\mathrm{CO}(2-1)]/L'[\mathrm{CO}(1-0)])^{-1}$. For $\alpha(2-1) = 1$, the molecular gas mass for GN26 is $M(\mathrm{H}_2) \simeq 7 \times 10^{10} M_{\odot}$.

The baryonic gas fraction provides an estimate of the evolutionary state of the system [$\mu \equiv M_{\mathrm{gas}}/(M_{\mathrm{gas}} + M_{\mathrm{stars}})$] (e.g., Frayer & Brown 1997). Massive local spirals have gas fractions of $\mu \simeq 0.05$–0.1 (Young & Scoville 1991), while younger gas-rich systems have higher gas fractions and more evolved systems have lower gas fractions. To derive the stellar mass and the gas fraction for GN26, we used the Bruzual & Charlot (2003) population synthesis models to fit the multi-wavelength (U through z-band and *Spitzer* IRAC 3-6μm) photometry. We assumed solar metallicities, a Salpeter IMF, and star-formation histories ranging from a single instantaneous burst to various *e*-folding timescales, including constant star-formation. We estimate an age of the stellar population of 1.3 Gyr and a total stellar mass of $(2.1 \pm 0.6) \times 10^{11}\,\mathrm{M}_{\odot}$ for an e-folding timescale of 1.0 Gyr. Neglecting HI ($M_{gas} \simeq M(\mathrm{H}_2)$), the implied gas fraction is $\mu = 0.25 \pm 0.10$.

The dynamical mass is highly uncertain given the lack of resolution of the CO data and the uncertain kinematics associated with the merger event. However, the CO size of $\theta(\mathrm{FWHM}) < 4''$ (diameter < 33 kpc) can provide a crude constraint on the dynamical mass. For a wide range of mass distributions, the dynamical mass can be approximated by $M_{\mathrm{dyn}} \approx R(\Delta V/[2\sin(i)])^2/G$, where ΔV is the observed FWHM line width, G is the gravitational constant, and i is the inclination. If the intrinsic axial ratio is about 1, the observed optical morphology implies an inclination of $i \simeq 40^{\circ}$. For a radius of $R < 16.5$ kpc, a CO line width of 560 km s^{-1}, and $i \simeq 40^{\circ}$, the dynamical mass is $M_{\mathrm{dyn}} < 7 \times 10^{11} M_{\odot}$. This result implies a gas-fraction of larger than 10% which is consistent with the estimate based on the stellar mass.

We derive a FIR (42.5–122.5 μm) luminosity of $L(\mathrm{FIR}) = (4.0 \pm 1.2) \times 10^{12} L_{\odot}$ and a total infrared luminosity (8–1000 μm)[11] of $L(\mathrm{IR}) = (5.6 \pm 1.7) \times 10^{12} L_{\odot}$, using the 70, 160, and 850 μm flux densities (Pope et al. 2006; Huynh et al. 2007) and the IRS spectrum (Pope et al.

---

[11] We adopt an IR definition of 8–1000 μm and the *IRAS* FIR definition of 42.5–122.5 μm throughout this paper.

2008). A single-temperature greybody with $T_d = 41 \pm 3\,$K and a dust-emissivity index of $\beta \simeq 2$ fit the data. Similar luminosities have been previously derived based on local spectral energy distribution (SED) templates (Huynh et al. 2007; Pope et al. 2008), but a simple greybody provides a better fit to the FIR data for this system.

4. DISCUSSION

GN26 has a disturbed, merger-like morphology (Fig. 1) similar to local ULIRGs and many high-redshift ULIRGs/SMGs. The *Spitzer* mid-infrared IRS spectrum (Pope et al. 2008), the infrared-to-radio flux density ratio (Huynh et al. 2007), and the X-ray emission (Alexander et al. 2005) are all consistent with GN26 being predominantly powered by star formation. The large CO(2→1) flux is consistent with this view.

We derive a total star-formation rate of $\mathrm{SFR} \simeq 950\,M_\odot\,\mathrm{yr}^{-1}$, using $\mathrm{SFR}(M_\odot\,\mathrm{yr}^{-1}) = 1.7 \times 10^{-10}\mathrm{L(IR)}/\mathrm{L}_\odot$ which assumes a Salpeter IMF (Kennicutt 1998). The $L(\mathrm{IR})/L'(\mathrm{CO})$ ratio provides an indication of the intensity of star-formation and star-formation efficiency. Strong starbursts and ULIRGs tend to show high IR-to-CO luminosity ratios of $\gtrsim 100$, while local spiral galaxies have lower values of about 10–50 (e.g., Solomon & Vanden Bout 2005). For GN26, $L(\mathrm{IR})/L'(\mathrm{CO}) = 80 \pm 30\ \mathrm{L}_\odot(\mathrm{K\,km\,s^{-1}\,pc^2})^{-1}$. An average ratio of 350 has been reported for high-redshift CO sources (Solomon & Vanden Bout 2005). However, previous $L(\mathrm{IR})$ estimates for the SMGs assume a temperature of 40 K (Greve et al. 2005), while multi-wavelength data suggest a lower average dust temperature of about 35 K for the SMG population (Chapman et al. 2005; Kovács et al. 2006; Pope et al. 2006, 2008; Huynh et al. 2007), implying a factor of two decrease in their luminosities. If adopting an average temperature of 35 K for the SMGs and placing the data on the same infrared luminosity scale, we find that both the high-redshift SMGs (Greve et al. 2005) and local ULIRGs (Solomon et al. 1997) have a similar average value of $L(\mathrm{IR})/L'(\mathrm{CO}) \simeq 200 \pm 100\,\mathrm{L}_\odot(\mathrm{K\,km\,s^{-1}\,pc^2})^{-1}$. The value for GN26 is on the low end of the range of values found for the more distant SMGs and local ULIRGs.

In comparison, the recent CO observations of the massive $z \sim 2$ BzK galaxies (galaxies selected on the basis of their $B - z$ and $z - K$ colors, Daddi et al. 2007) suggest a similar ratio of $L(\mathrm{IR})/L'(\mathrm{CO}) = 60 \pm 30\,\mathrm{L}_\odot(\mathrm{K\,km\,s^{-1}\,pc^2})^{-1}$ (Daddi et al. 2008). Although the IR-to-CO luminosity ratios for GN26 and the BzKs are similar, the BzKs are suspected to have much longer star-formation time scales. For the adopted CO-to-H_2 conversion factor ($\alpha[2-1] \simeq 1$), the estimated star-formation (gas consumption) time scale of $M(\mathrm{H}_2)/\mathrm{SFR} = 70\,$Myr for GN26 is consistent with a merger-driven starburst and the short time scales estimated previously for starbursts in local ULIRGs and distant SMGs (Solomon & Vanden Bout 2005; Tacconi et al. 2008). In contrast, the BzK are thought to have much longer star-formation time scales of order $\gtrsim 400\,$Myr based on their estimated duty cycle (Daddi et al. 2007). The gas consumption time scales for the BzKs based on the CO data would be consistent with these results if the Galactic CO-to-H_2 conversion factor is adopted for the BzKs (e.g., $\alpha(1-0) = 4.8\,M_\odot(\mathrm{K\,km\,s^{-1}\,pc^2})^{-1}$, Sanders et al. 1991). Within this paradigm, BzK galaxies would be analogous to local spirals with enhanced SFRs and long star-formation time scales, while the SMGs would be analogous to local ULIRGs with short time scales. However, such generalizations may be an over simplification. High-redshift galaxies such as GN26 and the BzKs may have a wide range of star-formation time scales between the intense short-lived starbursts found in local ULIRGs of order 10 Myr and the long time scales of order 1 Gyr found for local spirals. Future high-resolution CO observations are needed to constrain the CO-to-H_2 conversion factors and the associated gas consumption time scales before definitive conclusions may be drawn.

GN26 is not representative of most SMGs studied to date. It has a relatively low redshift, is faint at $850\,\mu$m, and is warmer than other SMGs detected at $z \sim 1$ (Chapman et al. 2005). It also has the largest observed S(CO)/S850 ratio of any SMG to date by a factor of 5 (in part due to the K-correction of this ratio). Previous high-redshift CO surveys have concentrated on the brightest $850\,\mu$m sources which are typically at $z > 2$. For sources at $z \sim 1$, the *Spitzer* 70 and $160\,\mu$m surveys and future Herschel surveys which probe the peak of the FIR SED may be more effective at identifying the brightest CO sources than the current $850\,\mu$m surveys. The relative importance of low-redshift SMGs ($z \sim 1$, Wang et al. 2006, 2008), "typical" SMGs ($2 \lesssim z \lesssim 3$, Blain et al. 2002; Chapman et al. 2005), and the most distant SMGs ($z > 3$, Dunlop et al. 2004; Wang et al. 2007; Younger et al. 2007, 2008; Dannerbauer et al. 2008) is an active topic of discussion. Wall et al. (2008) have recently argued for two distinct populations of SMGs: ULIRGs at $z \sim 1$ and more luminous ULIRGs at $z \sim$2–3. Comparing the CO properties of SMGs as a function of redshift and luminosity may help to test the hypothesis of multiple SMG populations.

5. CONCLUDING REMARKS

GN26 is a merger-driven starburst with a molecular gas mass of about $7 \times 10^{10} M_\odot$. Although it is the brightest FIR ($70\,\mu$m and $160\,\mu$m) high-redshift ($z > 1$) source in GOODS-North, it has not been previously observed in CO given that it is among the faintest $850\,\mu$m sources. The CO properties of GN26 are consistent with local ULIRGs and the high-redshift SMGs. The derived gas fraction of 0.25 ± 0.10 based on the stellar and molecular gas mass estimates suggests that about 75% of the available baryonic mass has already been converted into stars. Furthermore, at the current star-formation rate, the molecular gas will be depleted within $\lesssim 100$ Myr. The short gas consumption time scale for GN26 is in contrast to long time scales found for local spiral galaxies and estimates made for the high-redshift BzKs.

These observations represent the first discovery of high-redshift CO using CARMA. Planned improvements of the CARMA receivers will allow for CO observations of significant samples of distant ULIRGs discovered by the ongoing *Spitzer* programs and future Herschel surveys.

Support for CARMA construction was derived from the Gordon and Betty Moore Foundation, the Kenneth T. and Eileen L. Norris Foundation, the Associates of the California Institute of Technology, the states of California, Illinois, and Maryland, and the National Science Foundation. Ongoing CARMA development and operations are supported by the National Science Foundation under a cooperative agreement, and by the CARMA partner universities. This work is based in part on observations made with the *Spitzer* Space Telescope and has made use of the NASA/IPAC Extragalactic Database (NED), both of which are operated by the Jet Propulsion Laboratory, California Institute of Technology under a contract with NASA. The optical image was obtained from the Multimission Archive at the Space Telescope Science Institute (MAST).

REFERENCES

Alexander, D. M., Bauer, F. E., Chapman, S. C., Smail, I., Blain, A. W., Brandt, W. N., & Ivison, R. J. 2005, ApJ, 632, 736
Barger, A. J., Cowie, L. L., Sanders, D. B., Fulton, E., Taniguchi, Y., Sato, Y., Kawara, K., & Okuda, H. 1998, Nature, 394, 248
Blain, A. W., Smail, I., Ivison, R. J., Kneib, J.-P., & Frayer, D. T. 2002, Phys. Rep., 369, 111
Borys, C., Chapman, S., Halpern, M., & Scott, D. 2003, MNRAS, 344, 385
Bruzual, G., & Charlot, S. 2003, MNRAS, 344, 1000
Caputi, K. I., et al. 2007, ApJ, 660, 97
Chapman, S. C., Blain, A. W., Smail, I., & Ivison, R. J. 2005, ApJ, 622, 772
Chary, R., et al. 2004, ApJS, 154, 80
Cohen, J. G., Cowie, L. L., Hogg, D. W., Songaila, A., Blandford, R., Hu, E. M., & Shopbell, P. 1996, ApJ, 471, L5
Cowie, L. L., Barger, A. J., Hu, E. M., Capak, P., & Songaila, A. 2004, AJ, 127, 3137
Daddi, E., Dannerbauer, H., Elbaz, D., Dickinson, M., Morrison, G., Stern, D., & Ravindranath, S. 2008, ApJ, 673, L21
Daddi, E., et al. 2007, ApJ, 670, 156
Dannerbauer, H., Walter, F., & Morrison, G. 2008, ApJ, 673, L127
Downes, D., & Solomon, P. M. 1998, ApJ, 507, 615
Dunlop, J. S., et al. 2004, MNRAS, 350, 769
Frayer, D. T., et al. 2006, ApJ, 647, L9
Frayer, D. T., et al. 1999, ApJ, 514, L13
Frayer, D. T., Ivison, R. J., Scoville, N. Z., Yun, M., Evans, A. S., Smail, I., Blain, A. W., & Kneib, J.-P. 1998, ApJ, 506, L7
Frayer, D. T., & Brown, R. L. 1997, ApJS, 113, 221
Greve, T. R., et al. 2005, MNRAS, 359, 1165
Hughes, D. H., et al. 1998, Nature, 394, 241
Huynh, M. T., Pope, A., Frayer, D. T., & Scott, D. 2007, ApJ, 659, 305
Kennicutt, R. C., Jr. 1998, ARA&A, 36, 189
Kovács, A., Chapman, S. C., Dowell, C. D., Blain, A. W., Ivison, R. J., Smail, I., & Phillips, T. G. 2006, ApJ, 650, 592
Lagache, G., et al. 2004, ApJS, 154, 112
Le Floc'h, E., et al. 2005, ApJ, 632, 169
Neri, R., et al. 2003, ApJ, 597, L113
Papovich, C., et al. 2006, ApJ, 640, 92
Pope, A., et al. 2008, ApJ, in press (arXiv:0711.1553)
Pope, A., et al. 2006, MNRAS, 370, 1185
Sault, R. J., Teuben, P. J., & Wright, M. C. H. 1995, Astronomical Data Analysis Software and Systems IV, 77, 433
Sanders, D. B., Scoville, N. Z., & Soifer, B. T. 1991, ApJ, 370, 158
Smail, I., Ivison, R. J., & Blain, A. W. 1997, ApJ, 490, L5
Solomon, P. M., & Vanden Bout, P. A. 2005, ARA&A, 43, 677
Solomon, P. M., Downes, D., Radford, S. J. E., & Barrett, J. W. 1997, ApJ, 478, 144
Tacconi, L. J., et al. 2008, ApJ, in press (arXiv:0801.3650)
Tacconi, L. J., et al. 2006, ApJ, 640, 228
Wall, J. V., Pope, A., & Scott, D. 2008, MNRAS, 383, 435
Wang, W.-H., Cowie, L. L., & Barger, A. J. 2008, Ap&SS, 313, 317
Wang, W.-H., Cowie, L. L., van Saders, J., Barger, A. J., & Williams, J. P. 2007, ApJ, 670, L89
Wang, W.-H., Cowie, L. L., & Barger, A. J. 2006, ApJ, 647, 74
Wirth, G. D., et al. 2004, AJ, 127, 3121
Young, J. S., & Scoville, N. Z. 1991, ARA&A, 29, 581
Younger, J. D., et al. 2008, MNRAS, submitted (arXiv:0801.2764)
Younger, J. D., et al. 2007, ApJ, 671, 1531

TABLE 1

CO(2→1) OBSERVATIONAL RESULTS

Parameter	Value
α(J2000)	$12^{\mathrm{h}}36^{\mathrm{m}}34\overset{\mathrm{s}}{.}51 \pm 0\overset{\mathrm{s}}{.}08$
δ(J2000)	$+62^{\circ}12'41\overset{''}{.}2 \pm 0\overset{''}{.}5$
z(CO)	1.2234 ± 0.0007
Linewidth (FWHM)	$560 \pm 90\,\mathrm{km\ s^{-1}}$
S(CO)[a]	$3.45 \pm 0.93\,\mathrm{Jy\,km\ s^{-1}}$
L(CO)	$(2.7 \pm 0.7) \times 10^{7} h_{70}^{-2} L_{\odot}$
L'(CO)	$(6.8 \pm 1.8) \times 10^{10} h_{70}^{-2}\,\mathrm{K\,km\ s^{-1}\ pc^{2}}$
$M(\mathrm{H_2})$[b]	$7 \times 10^{10} h_{70}^{-2} M_{\odot}$

[a] Observed total CO(2→1) line flux. Uncertainty includes the 14% systematic calibration uncertainty and the 13% (7.5σ detection) random noise.

[b] Estimated assuming $\alpha(2-1) = 1\,M_{\odot}(\mathrm{K\,km\ s^{-1}\ pc^{2}})^{-1}$.

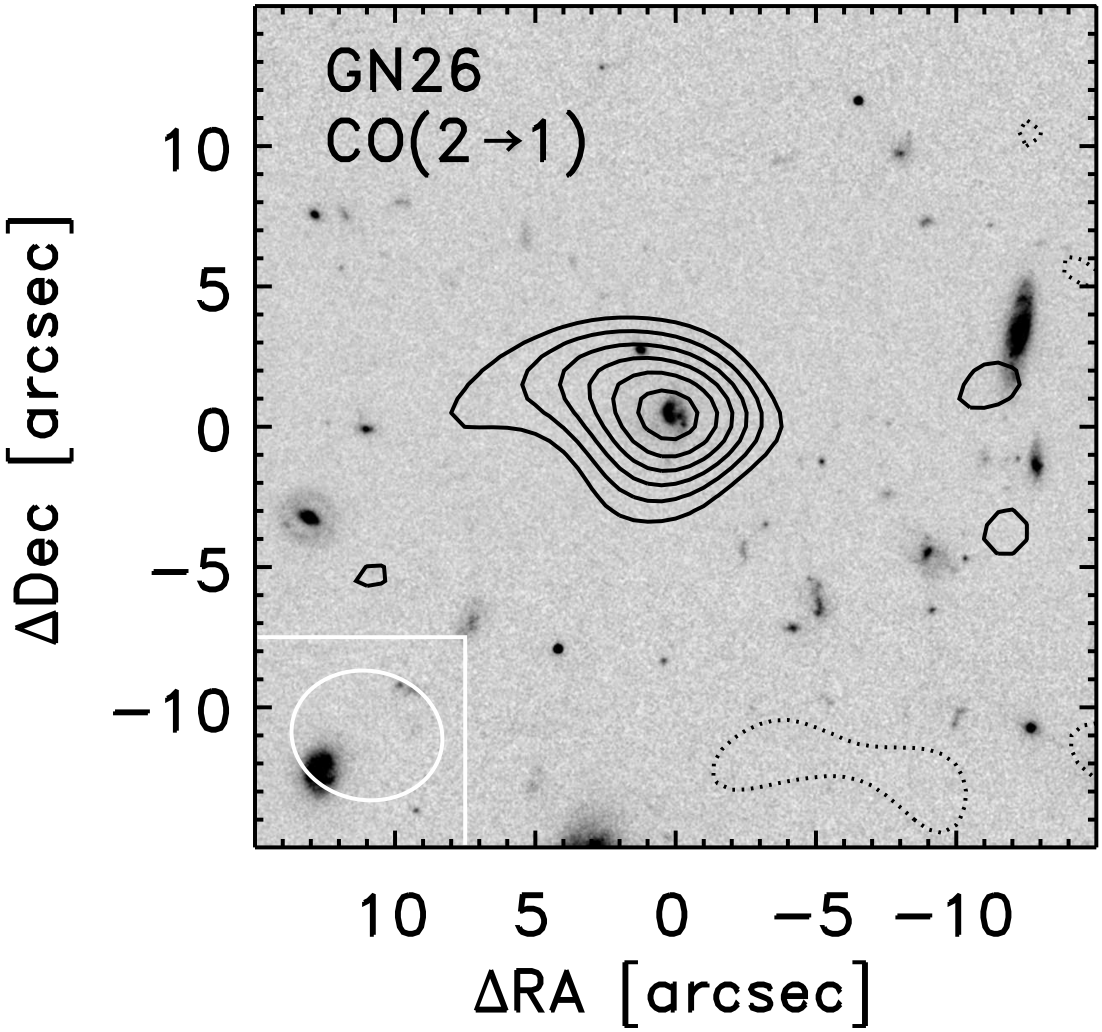

FIG. 1.— The integrated CO(2→1) map of GN26 averaged over 312.5 MHz (904 km s^{-1}) overlaid on an optical *HST*-ACS *z*-band image (grey-scale). The 1σ error is 0.46 Jy km s^{-1}/beam, and the contour levels are $1\sigma\times(-2,2,3,4,5,6,7)$; positive contours are solid lines and negative contours are dotted lines. The synthesized beam size (white ellipse) for the observations is shown in the lower left ($5''.4 \times 4''.6, \mathrm{PA} = 80^{\circ}$).

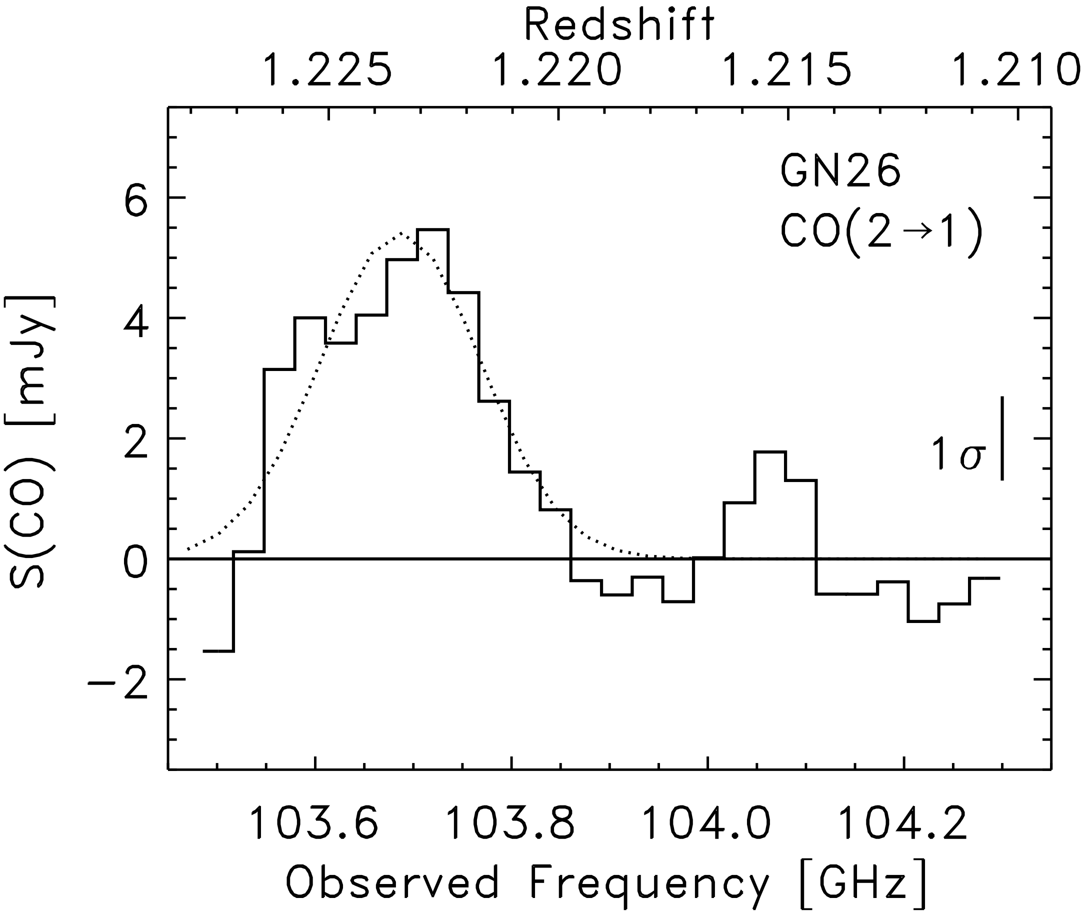

FIG. 2.— The CO(2→1) spectrum for GN26. The spectrum has been Hanning-smoothed. The channel increment is 31.25 MHz (90.4 km s^{-1}), and the 1σ error bar per smoothed channel is shown to the right. The dotted-line shows a Gaussian fit of the line profile for the unsmoothed data.